



In-situ

ff



K. C., W., L.* , L. H., C., L., W., K. E., L. L., G., T. P.

Gemological Institute, China University of Geosciences, Wuhan 430074, PR China
 Hubei Gem and Jewelry Engineering Technology Research Center, Wuhan 430074, PR China
 School of Materials Science and Engineering, Huazhong University of Science and Technology, Wuhan 430074, PR China
 Mechanical Engineering, University of Birmingham, Birmingham B15 2TT, UK
 School of Electrical and Electronic Engineering, Huazhong University of Science and Technology, Wuhan 430074, PR China
 WMG, Materials Engineering Centre, University of Warwick, CV4 7AL Coventry, UK

ARTICLE INFO

ABSTRACT

Keywords:

T
C
S
C
E

C (3DG) w
w H w
(SLM)
G w in-situ w (CVD) C
3DG A w CVD w
SLM ff 3DG (
ff T 3DG/ ff 88% 27%
(EMI) ff P EMI ffi
(SE) 47.8 B 2.7 GH SE 32.3 B 2–18 GH
T SLM

1. Introduction

G sp^2
w
($2630 \text{ cm}^{-2} \text{ V}^{-1}$) 1
($2 \times 10^5 \text{ W}^{-1} \text{ K}^{-1}$) 2. H w
w (2D) ff
3. A fi ff
C w
(3DG) w (99.7%), w
fi (0.6 cm^{-2}) 4 w fi w
w w

(2DG), 5, 6,7
4, (EMI) 8
V 3DG
9, 10,
11, 12 H w
F
ff 13. S
() w
14. D w
15. M
CVD w
16. B
w w
w

*C : G I , C U G , W 430074, PR C .
E-mail address: @ (. L).

. T (, fi
) , fl fi
(,) 3DG. B
3DG w
(,). H w
ffi
N
3DG w
fi 17,18
H , w
3DG w
19
S (SLM),
(AM)
(3D)
w ffi
fl *in-situ* T
SLM T 20
21 , N 22 . C w
C w N
w
CVD w (< 0.001 %)
w , w
23 . W N
(> 0.1 %) 17 , fi
24 . H w
SLM ffi
w
fl w w
(1000–1100). F ff
SLM 25
T , w fi
3DG/ (3DG/C)
SLM w CVD w
A w
SLM

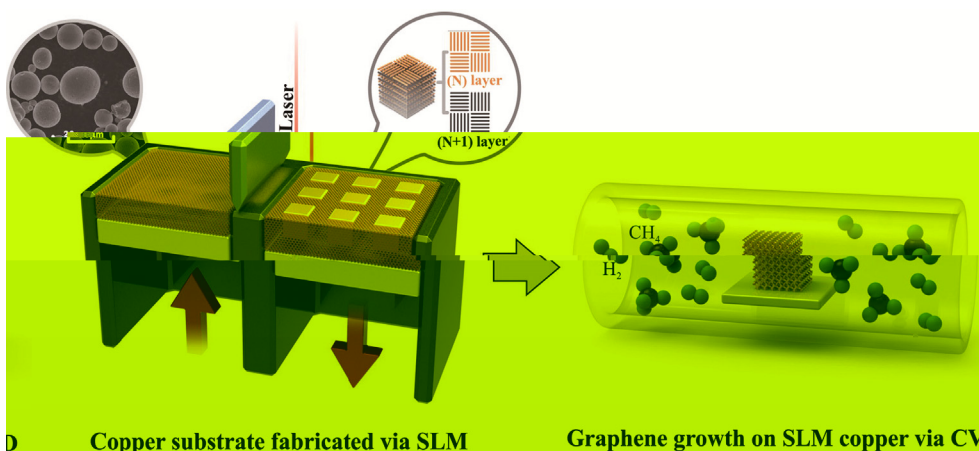


Fig. 1. (a) Schematic of the SLM process for copper substrate fabrication and subsequent in-situ CVD growth of graphene on the SLM copper substrate.

ASTMB193-2002 (Tensile strength) and ASTM E1461-2013 (Tensile strength) were used as reference standards for mechanical properties. The tensile strength of the SLM copper substrate was measured using a universal testing machine (LFA 457, G1010) with a load cell (SENTERRA, B1000) and a crosshead speed of 0.5 mm/min. The tensile strength of the SLM copper substrate was measured using a universal testing machine (LFA 457, G1010) with a load cell (SENTERRA, B1000) and a crosshead speed of 0.5 mm/min. The tensile strength of the SLM copper substrate was measured using a universal testing machine (LFA 457, G1010) with a load cell (SENTERRA, B1000) and a crosshead speed of 0.5 mm/min. The tensile strength of the SLM copper substrate was measured using a universal testing machine (LFA 457, G1010) with a load cell (SENTERRA, B1000) and a crosshead speed of 0.5 mm/min. The tensile strength of the SLM copper substrate was measured using a universal testing machine (LFA 457, G1010) with a load cell (SENTERRA, B1000) and a crosshead speed of 0.5 mm/min.

3. Results and discussion

3.1. Formation of SLM copper

3.1.1. SLM manufacturing of copper under different line energy densities

The SLM process was performed under different laser power and scanning speed conditions to study the effect of line energy density on the surface morphology and mechanical properties of the SLM copper substrate.

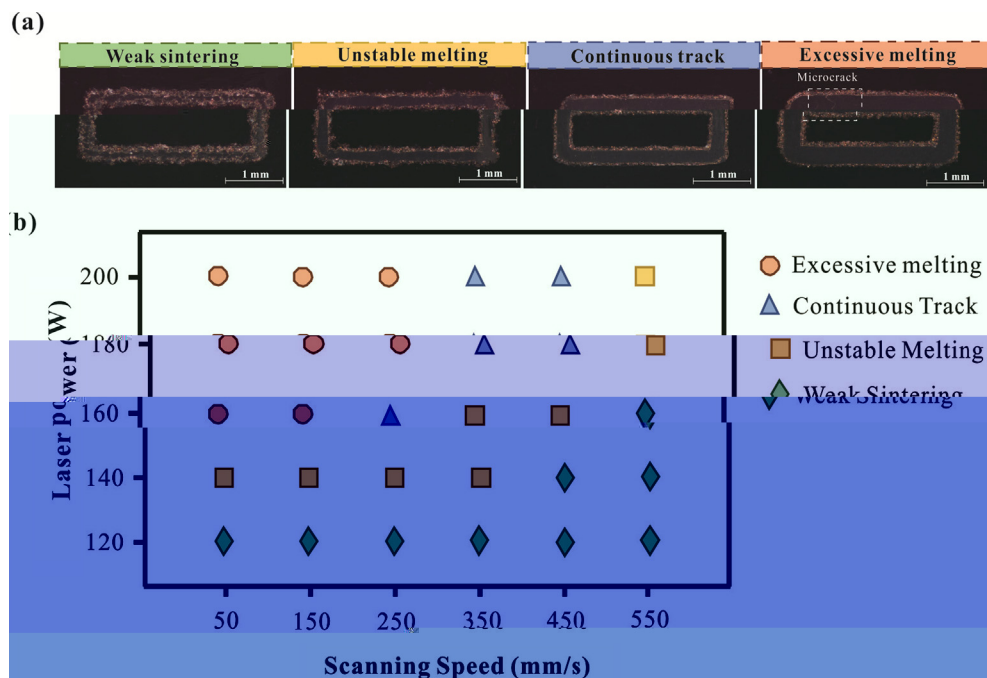


Fig. 2. (a) SEM images of SLM copper substrate surfaces under different laser power and scanning speed conditions: Weak sintering, Unstable melting, Continuous track, and Excessive melting. (b) Scatter plot of Laser Power (W) vs Scanning Speed (mm/s) showing the regions for Excessive melting, Continuous Track, Unstable Melting, and Weak Sintering.

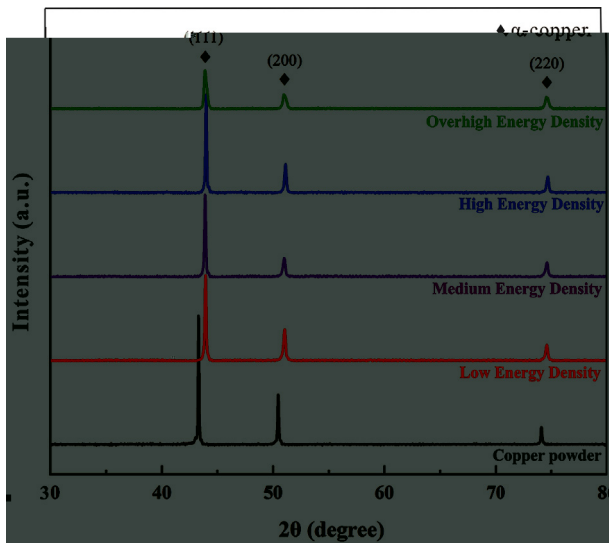


Fig. 3. RD patterns of copper powder at different energy densities: (a) 3000 J/mm³, (b) 857 J/mm³, (c) 128 J/mm³, and (d) 285 J/mm³.

3.1.2. Formation of anisotropic microstructure under different volumetric energy density

The XRD patterns of copper powder at different energy densities are shown in Fig. 3. The intensity of the (111) peak is significantly higher than that of the (200) and (220) peaks at 3000 J/mm³ (Fig. 3a), indicating a strong preferred orientation along the [111] direction. As the energy density decreases to 857 J/mm³ (Fig. 3b), the intensity of the (111) peak decreases, and the (200) and (220) peaks become more prominent. At 128 J/mm³ (Fig. 3c) and 285 J/mm³ (Fig. 3d), the XRD patterns show a more random orientation of the copper powder particles, with the (111) peak intensity being much lower than at 3000 J/mm³.

The SEM micrographs of the copper powder particles at different energy densities are shown in Fig. 4. At 3000 J/mm³ (Fig. 4a), the particles are highly oriented along the [111] direction, forming a dense, layered structure. At 857 J/mm³ (Fig. 4b), the particles are less oriented and more randomly distributed. At 128 J/mm³ (Fig. 4c), the particles are highly oriented along the [111] direction, forming a dense, layered structure. At 285 J/mm³ (Fig. 4d), the particles are less oriented and more randomly distributed. The SEM micrographs show that the particles are highly oriented along the [111] direction at 3000 J/mm³ and 128 J/mm³, while they are less oriented at 857 J/mm³ and 285 J/mm³. The SEM micrographs also show that the particles are highly oriented along the [111] direction at 3000 J/mm³ and 128 J/mm³, while they are less oriented at 857 J/mm³ and 285 J/mm³.

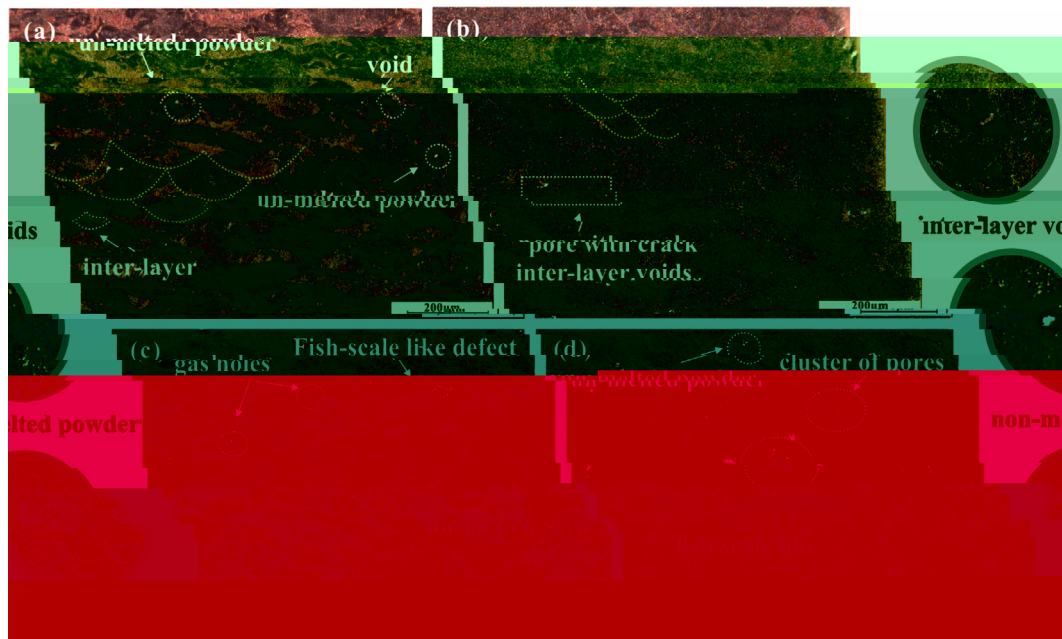


Fig. 4. SEM micrographs of copper powder particles at different energy densities: (a) 3000 J/mm³, (b) 857 J/mm³, (c) 128 J/mm³, and (d) 285 J/mm³.

... ..

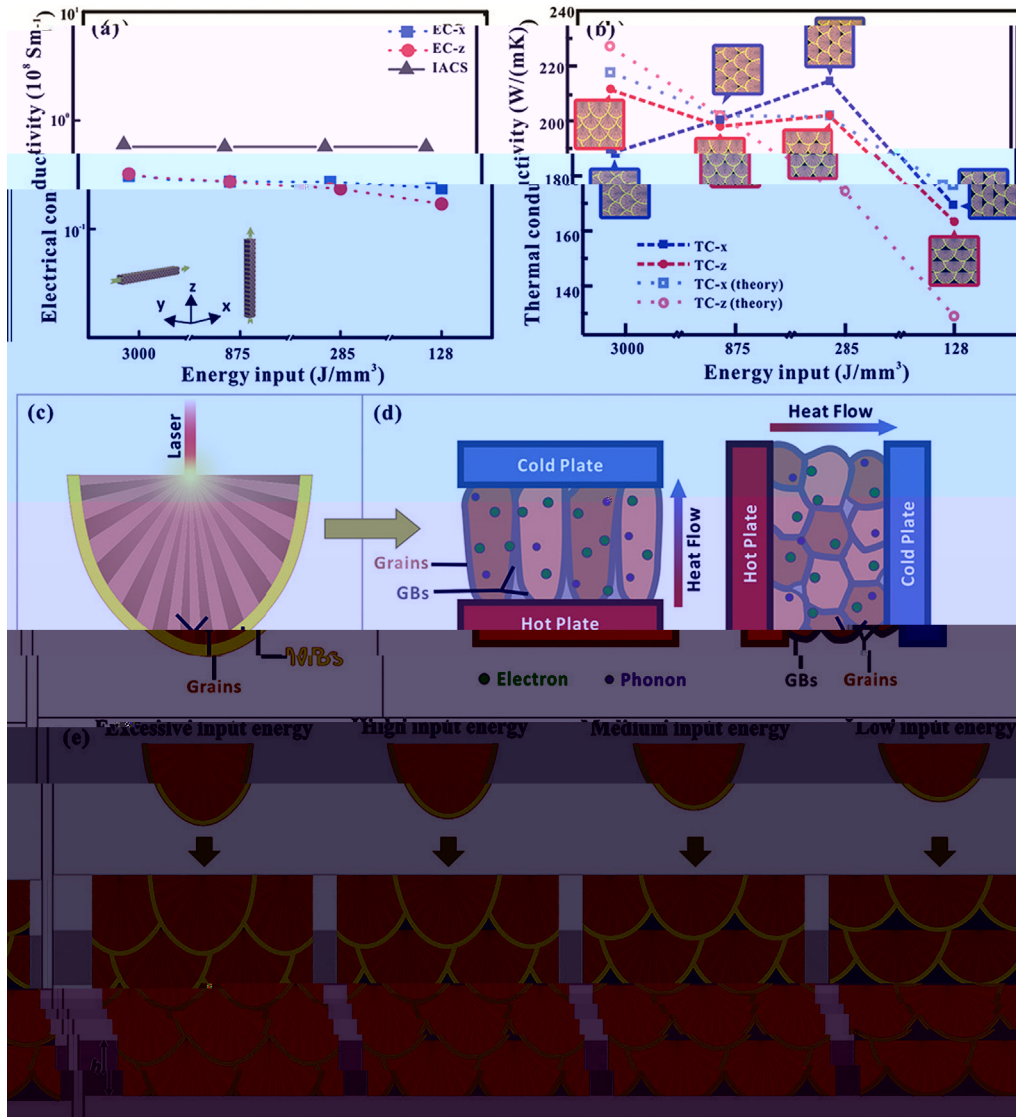


Fig. 7. (a) Electrical conductivity of EC-x, EC-z and IACS as a function of energy input. (b) Thermal conductivity of TC-x, TC-z and theoretical values as a function of energy input. (c) Schematic diagram of laser irradiation on a material. (d) Schematic diagram of heat flow through grains and grain boundaries (GBs) between hot and cold plates. (e) Cross-sectional diagrams showing grain growth under different energy input levels: excessive, high, medium, and low.

SEM, with a magnification of 5000 \times . The average grain size of the 3DG/C is approximately 450 μm (Fig. 8a). A cross-sectional SEM image of the 3DG/C is shown in Fig. 8b, which reveals a porous structure with a large surface area. The EDS analysis of the 3DG/C is shown in Fig. 8c-d, which indicates the presence of carbon and copper. The SEM image of the 3DG/C is shown in Fig. 8e-g. The SEM image of the 3DG/C is shown in Fig. 8h.

3.3. Morphology and structure of CVD 3DG/Cu porous scaffolds

The morphology and structure of the CVD 3DG/Cu porous scaffolds were investigated using SEM. The SEM image of the 3DG/Cu porous scaffold is shown in Fig. 8a, which reveals a porous structure with a large surface area. The average grain size of the 3DG/Cu porous scaffold is approximately 450 μm . A cross-sectional SEM image of the 3DG/Cu porous scaffold is shown in Fig. 8b, which reveals a porous structure with a large surface area. The EDS analysis of the 3DG/Cu porous scaffold is shown in Fig. 8c-d, which indicates the presence of carbon and copper. The SEM image of the 3DG/Cu porous scaffold is shown in Fig. 8e-g. The SEM image of the 3DG/Cu porous scaffold is shown in Fig. 8h.

The morphology and structure of the CVD 3DG/Cu porous scaffolds were investigated using SEM. The SEM image of the 3DG/Cu porous scaffold is shown in Fig. 8a, which reveals a porous structure with a large surface area. The average grain size of the 3DG/Cu porous scaffold is approximately 450 μm . A cross-sectional SEM image of the 3DG/Cu porous scaffold is shown in Fig. 8b, which reveals a porous structure with a large surface area. The EDS analysis of the 3DG/Cu porous scaffold is shown in Fig. 8c-d, which indicates the presence of carbon and copper. The SEM image of the 3DG/Cu porous scaffold is shown in Fig. 8e-g. The SEM image of the 3DG/Cu porous scaffold is shown in Fig. 8h.

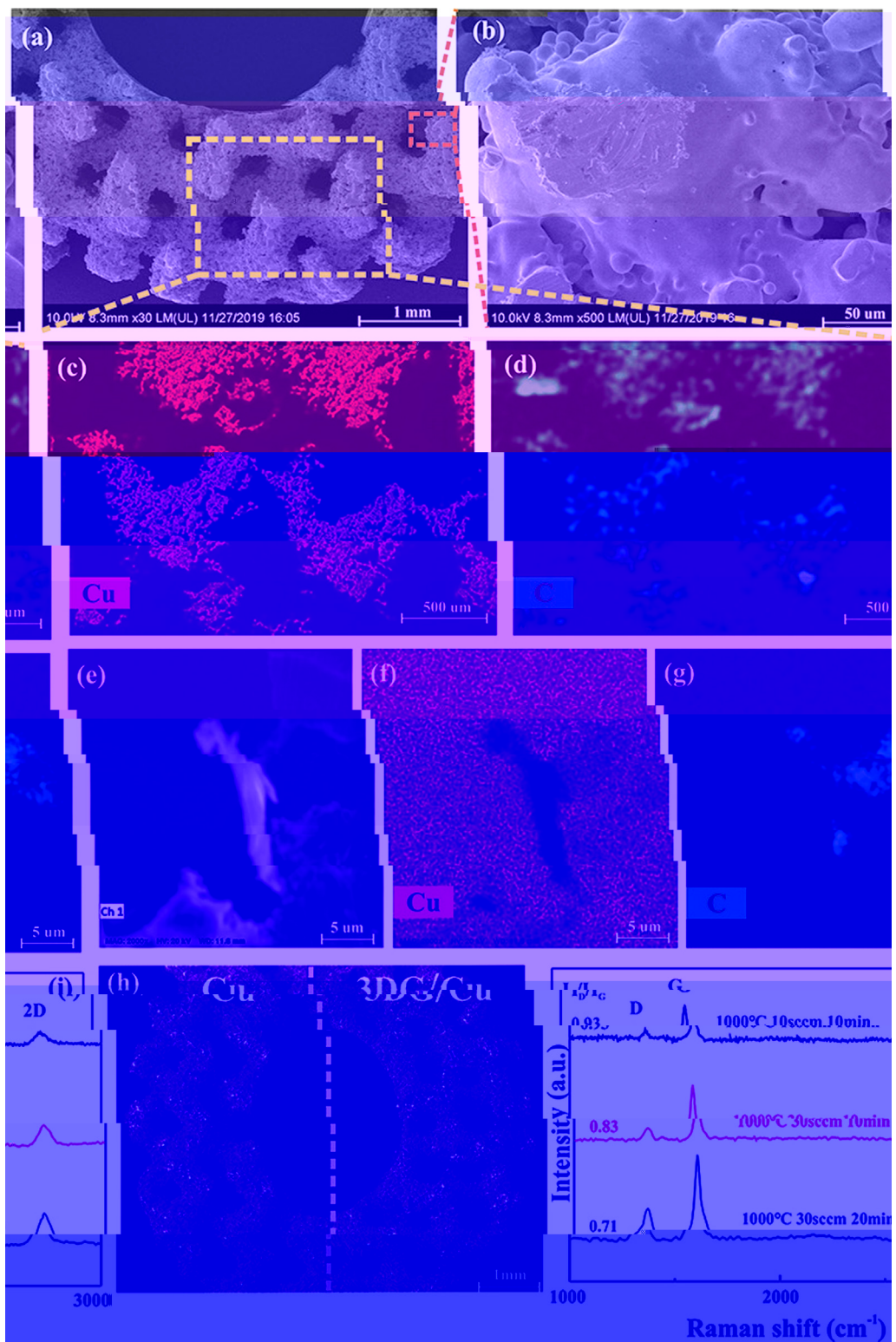


Fig. 8. (a) SEM image of 3DG/C porous scaffold; (b) SEM image of 3DG/C porous scaffold; (c) EDS map of Cu; (d) EDS map of C; (e) SEM image of 3DG/C porous scaffold; (f) EDS map of Cu; (g) EDS map of C; (h) EDS maps of Cu and 3DG/Cu; (i) Raman spectra of 3DG/C porous scaffolds after 1000°C 10secm 10min, 1000°C 30secm 10min, and 1000°C 30secm 20min.

W_D = 0.93, W_G = 0.07, I_D/I_G = 0.71. The Raman spectra of 3DG/C porous scaffolds after 1000°C 10secm 10min, 1000°C 30secm 10min, and 1000°C 30secm 20min are shown in Fig. 8(i). The Raman spectra show the characteristic bands of 3DG/C porous scaffolds, including the 2D band at approximately 2700 cm⁻¹, the D band at approximately 1350 cm⁻¹, and the G band at approximately 1500 cm⁻¹. The intensity ratio of the D band to the G band (I_D/I_G) is 0.93, 0.83, and 0.71 for the 1000°C 10secm 10min, 1000°C 30secm 10min, and 1000°C 30secm 20min conditions, respectively.

3.4. Thermal property and EMI shielding effectiveness of 3DG/Cu porous scaffolds

The thermal stability of 3DG/Cu porous scaffolds was evaluated by TGA. The TGA curves of 3DG/Cu porous scaffolds after 1000°C 10secm 10min, 1000°C 30secm 10min, and 1000°C 30secm 20min are shown in Fig. 9. The TGA curves show that the 3DG/Cu porous scaffolds have a high thermal stability, with a weight loss of approximately 26.8% and 14.8% at 1000°C for the 1000°C 10secm 10min and 1000°C 30secm 10min conditions, respectively.

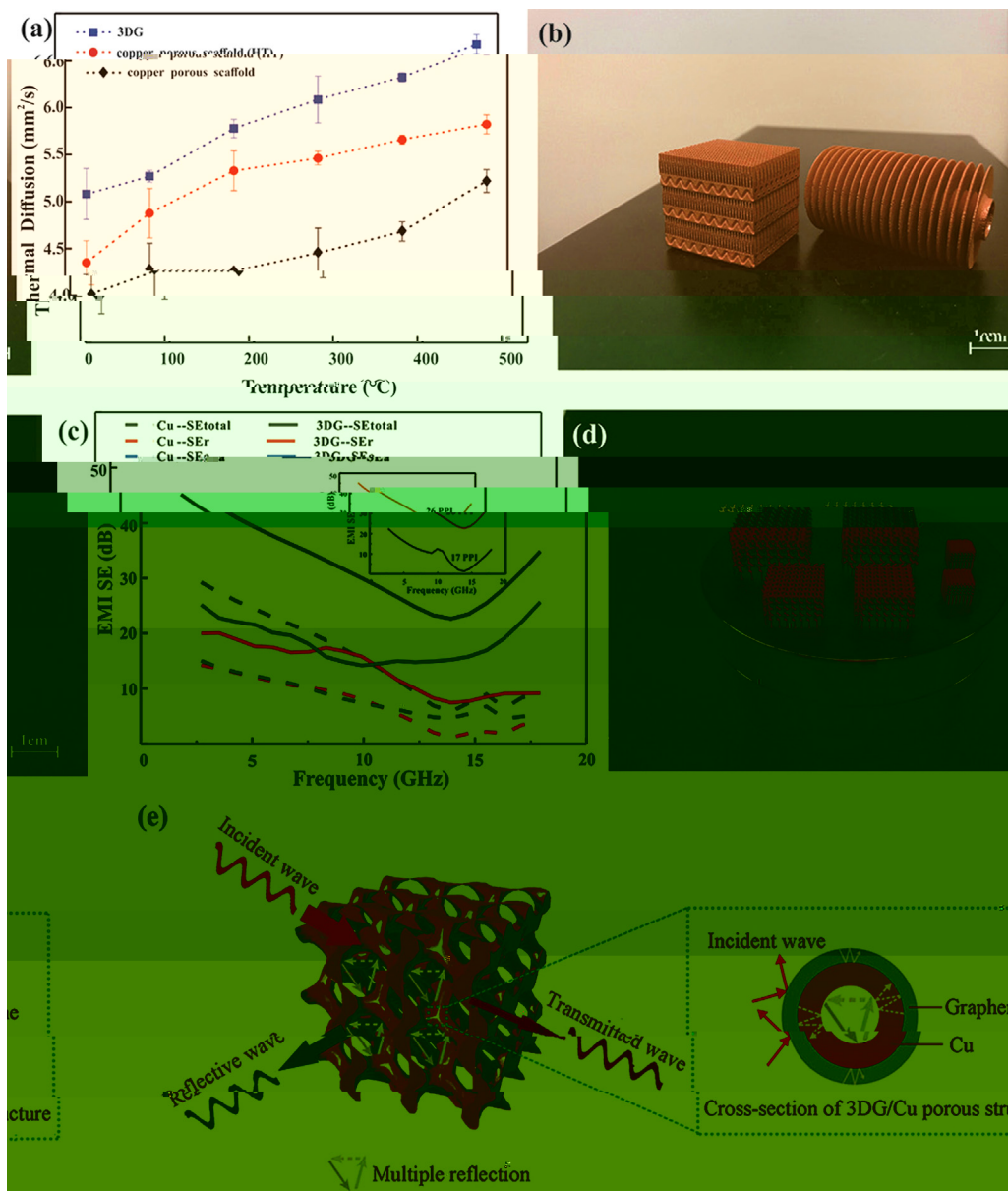


Fig. 9. (a) Thermal Diffusion of 3DG/Cu porous scaffold (□), copper porous scaffold (○) and copper porous scaffold@HTO (◇) (w/HTO) (○) SLM. (b) 3D models of 3DG and copper porous scaffold. (c) EMI SE of Cu-SEtotal (—), Cu-SEr (---), 3DG-SEtotal (—) and 3DG-SEr (---) of 3DG/Cu porous structure. (d) SEM image of 3DG/Cu porous structure. (e) Schematic of wave interaction with the porous structure. (w/HTO) (○) SLM. (□) 3DG/Cu porous structure. (○) copper porous scaffold. (◇) copper porous scaffold@HTO. (—) EMI SEtotal; (---) EMI SEr.

Table 1

Comparison of EMI shielding efficiency and thermal property improvement of various porous structures.

Coating materials	Substrate	Method	Maximum shielding efficiency (dB)	Improvement of thermal property (%)	Ref
G.	G.	I.	37	—	50
G.	PS	H.	29.3	—	56
G.	PMMA	S.	19	—	57
C /G.	A	S.	—	8.5	58
G.	N.	F.	—	554	59
G.	C-N.	E.	20	—	60
G.	C	P w.	—	2.4	61
G.	C	F.	47	6.3	62
G.	C	CVD + SLM	47.8	27	T

Note: (□) -PPMA, (○) -PS.

HT
in-situ w (F. 9a). S
 3DG/C ff
 HT
 1-2
 W
 SLM
 fl w (w fl) 500 μm
 (F. 9b),
 G
 (T. 1). I
 O
 T
 EMI, EMI SE, w 3DG/C ff
 (EM) w
 2-18 GHz (F. 9c),
 W *in-situ* w
 ff SE 15.9 32.3 B, w
 47.8 B (88.2%),
 20 B. T
 3DG/C fi w
 J K 44 EMI
 w T EMI SE
 133%) 20 110 PPI ().
 R K 45 EMI
 W
 17 26 PPI (F. 9c insert) 105%
 EMI SE. I w EMI
 ff w SLM. T
 3DG/C 26 PPI EMI SE
 32.3 B, 99.9% EMI w T
 60
 (30 ff) 46 T EMI
 3DG/C w
 T 1. I EMI SE
 3DG/C w
 3D
 T EMI fl (SE_r),
 (SE_a) fl (EM) w 47,
 w
 48 R 49 w
 w, w
 T w EM w
 fi
 50 R EMI
 T
 w w w
 w fi C 51 F
 w
 52 S O₂ 53 W
 3DG/C ff w

SE_r, SE_a, w F. 9e. W w
 w 3DG/C ff
 w w fl w ff S
 3DG/C
 fi
 w w T
 EM w fi w w
 w EM w
 SE_r, O
 w ff, w w fi EM
 w ff EM
 T
 ff w
 w J 54 I w
 fi w
 fl ff M
 w
 w fl
 EM w
 EM w T w
 w 44 T
 w 3D EM w w
 I CVD
 R S 3.3
 EM w w
 55 I
 O w
 3DG/C
 fi w fi
 T
 w ff

4. Conclusions

A 3DG/C ff w
in-situ CVD
 T ff W 3DG/C
 EMI SE
 15.9 () 32.3 B,
 47.8 B (88.2%), w 26.8%
 ff T 3DG/C
 ff fl fi
 T EMI
 3DG/C ff
 EMI

Credit authorship contribution statement

Kaka Cheng: C, M, F
 Wei Xiong: V, I, W
 Yan Li: W &, F
 Liang Hao: F
 Chunze Yan: R, F
 Zhaoqing Li: V
 Zhufeng Liu: F
 Yushen Wang: I, S
 Khamis Essa: W &
 Li Lee: D
 Xin Gong: S
 Ton Peijs: W &, S

Declaration of Competing Interest

T... fl...

Acknowledgement

T... w... fi... N... S... F... C... (N... 51671091, N... 51902295, N... 51675496). T... F... R... F... C... U... C... U... G... (W...) (N... CUG170677), H... P... N... S... F... (N... 2019 CFB264).

Appendix A. Supplementary data

S... // /10.1016/... 2020.105904.

References

1 B... N... N... M... K... M... S... G... ACS N... 2018;91:24-69.

2 B... AA, G... S, B... W, C... L, T... W... D, M... F... S... ACS N... 2008;8(3):902-7.

3 L... H, C... M, P... w... H, P... O, S... G... ACS A... M... I... 2016;8(36):24112-22.

4 K... M, K... J, J... B, C... K... JH, A... JH, G... ACS N... 2017;11(8):7950-7.

5 P... C... M, H... M, T... M... L... D... P... ACS N... 2020;262:118266-76.

6 L... J... W, C... LL, J... SH, W... G... L... F... C-G... ACS N... 2017;101:50-8.

7 H... Q, L... SW, C... LH, J... SH, H... H... Q... S... ACS N... 2018;6(42):21216-24.

8 D... TM, S... P, D... P, K... J, Kw... M, A... T... ACS N... 2017;1(4):467-70.

9 Q... L, L... L... T... ACS A... 2014;4(72):38273-80.

10 D... H... L... SP, N... W... JG... 3D... ACS N... 2016;90:424-32.

11 L... L... W, S... CO, H... MK, HL, D... W... ACS N... 2018;100:201803938.

12 L... J, P... C, R... G... N... D... G... ACS N... 2013;7(7):6001-6.

13 J... SH, A... w... S, G... A... L... ACS N... 2017;56:15520-38.

14 I... T... S... w... K, K... M, T... T... T... K... ACS N... 2018;20(9):6024-33.

15 S... K, D... N, M... C, V... N, E... J... T... ACS N... 2002;149(8):370-7.

16 C... H, S... M, S... WH, L... G, H... Q... ACS N... 2011;7(22):3163-8.

17 K... H, G... M, J... I, H... J, W... C, C... M... U... ACS N... 2019;1(4):1077-87.

18 S... Q... F... L, W, L... H, L... ACS N... 2017;29(31):1701583-90.

19 G... C... L... T... H... D, W... ACS N... 2019; // /10.1021/... 9 08191.

20 C... C, H... B... N... J, C... S, L... F... ACS N... 2019;175:107824-33.

21 S... ě... J, B... ě... D... T... ff... ACS N... 2016;307:407-17.

22 R... DC, HB, L... J, L... SJ, J... W... ACS N... 2020;771:138586-95.

23 L... C... W, A... J, K... S, N... J... ACS N... 2009;324(5932):1312-4.

24 C... P, R... WC, G... LB, L... BL, P... SE, C... HM... ACS N... 2011;10:424-8.

25 J... SD, D... S, G... L, K... JP, H... JV, V... ACS N... 2019;270:47-58.

26 W... H... L... L... T... D, C... Q, F... ACS N... 2019;170:107697-708.

27 G... DD, M... W, W... K, P... ACS N... 2013;57(3):133-64.

28 L... E, T... S, C... L, F... ACS N... 2017;249:255-63.

29 S... W... L... J, W... P, C... ACS N... 2018;124:685-98.

30 L... M... S, D... W, S... C... ACS N... 2015;87:797-806.

31 L... CLA, M... S, T... w... M, A... w... RC, W... PJ, L... PD... ACS N... 2019;166:294-305.

32 T... K... T... WQ, T... J, D... M, M... D... ACS N... 2016;6:26039-48.

33 K... H, T... P, L... NH, T... SB, C... CK... ACS N... 2016;11(3):183-91.

34 R... fi... HK, K... NV, G... H, S... TL, S... ACS N... 2013;22(12):3872-83.

35 T... K... T... J, V... G, P... Q... ACS N... 2015;646:303-9.

36 R... DA, M... LE, M... H... ACS N... 2011;59(10):4088-99.

37 W... H... ACS N... 2018;743:258-61.

38 K... S... W... ACS N... 2003;23:309-48.

39 L... G... G... J... ff... R... G... ACS N... 2010;10(9):3512-6.

40 L... S... C... WW, C... L... R... ff... R... ACS N... 2009;9(12):4268-72.

41 W... C... W... H... S... Q... ACS N... 2020;161:479-85.

42 F... AC, M... JC, S... V... C... C... L... M... M... F... ACS N... 2006;97(18):187401-4.

43 S... G... J... SH, F... PC, H... HQ... ACS N... 2017;200:97-100.

44 J... K... H... J... C... J... D... ACS N... 2014;311:351-6.

45 R... K... M... DP, A... C... M... S... S... K... E... ACS N... 2018;12:475-84.

46 S... B... L... W... W... C... ACS N... 2016;8(12):8050-7.

M 2019;34(5):489–98.

53 W B, C M, L M. R [https://doi.org/10.1016/j.compositesa.2014.06.011](#). *Composites Part A* 2014;26:3484–9.

54 C H, W S, J L, C J, S J. *Composites Part A* 2019;121:139–48.

55 W L, J Q, T ff MWCNT *Journal of Materials Science: Materials in Electronics* 2015;26(3):1895–9.

56 D P, GR, H P, Q F, M B, ML. *Efficient* *Journal of Materials Science: Materials in Electronics* 2012;22:18772–4.

57 HB, Q, WG, H, T *ACS Applied Materials Interfaces* 2011;3:918–24.

58 S A, U N, T V. T *Journal of Materials Science: Materials in Electronics* 2016. [https://doi.org/10.1051/comp/2016021](#).

59 P MT, J H, R ff RS, S L. T *Journal of Materials Science: Materials in Electronics* 2012;12:2959–64.

60 J K, H, H, D P *Composites Part A* 2017;122:244–7.

61 R H, L S, B S, K TW, L DS, L HJ, T *Journal of Materials Science: Materials in Electronics* 2015. [https://doi.org/10.1038/nmat42710](#).

62 T, F SG, L G, Q, L G, R KP, S *Journal of Materials Science: Materials in Electronics* 2020. [https://doi.org/10.1016/j.jmse.2019.105670](#).

63 R DA, M LE, M E, H DH, M JL, M BI, N *Journal of Materials Science: Materials in Electronics* 2011;59(10):4088–99.

64 E SF, L KG, S VK, M IC. T *Journal of Materials Science: Materials in Electronics* 1973;1(1):10–38.